# Electronic Structure of Chalcopyrite Surfaces for Photoelectrochemical Hydrogen Production

James C. Carter,[1,#] Dirk Hauschild,[1,2,3] Lothar Weinhardt,[1,2,3] Kimberly Horsley[4], Dimitrios Hariskos[5], Nicolas Gaillard,[4] and Clemens Heske[1,2,3,*]

[1] Department of Chemistry and Biochemistry, University of Nevada Las Vegas (UNLV), 4505 Maryland Parkway, Las Vegas, Nevada, 89154-4003, United States

[2] Institute for Photon Science and Synchrotron Radiation (IPS), Karlsruhe Institute of Technology (KIT), Hermann-v.-Helmholtz-Platz 1, 76344 Eggenstein-Leopoldshafen, Germany

[3] Institute for Chemical Technology and Polymer Chemistry (ITCP), Karlsruhe Institute of Technology (KIT), Engesserstr. 18/20, 76128 Karlsruhe, Germany

[4] Hawaii Natural Energy Institute (HNEI), University of Hawaii at Manoa, Honolulu, Hawaii, 96822, United States

[5] Zentrum für Sonnenenergie- und Wasserstoff-Forschung Baden-Württemberg (ZSW), Meitnerstraße 1, 70563 Stuttgart, Germany

*Corresponding author: heske@unlv.nevada.edu

## ABSTRACT

The electronic surface level positions of different chalcopyrite [$Cu(In,Ga)(S,Se)_2$] thin-film absorbers are presented and their suitability for photoelectrochemical (PEC) water splitting is discussed. For efficient PEC water splitting, electrode surfaces must exhibit suitable band edge energies (i.e., the conduction band minimum, CBM, and the valence band maximum, VBM) to enable hydrogen and oxygen evolution. The VBM and CBM at the sample surfaces were experimentally derived under vacuum conditions using direct and inverse photoemission. By measuring the work function at the surface, the band edge energies can be correlated to the normal hydrogen electrode (NHE) and compared with the reduction and oxidation potentials necessary to drive PEC water splitting. By studying several chalcopyrite variants differing in growth process,

composition, stoichiometry, and surface treatment, strategies are derived to optimize chalcopyrite PEC devices with respect to the redox potentials for solar water splitting.

## INTRODUCTION

Photoelectrochemical water splitting (PEC) uses two very abundant natural resources, water and sunlight, to produce hydrogen and oxygen gases, making it a very attractive pathway for producing sustainable fuels.[1–4] However, in order for PEC to become a viable solution to the world's ever-growing energy demands, several important milestones must be reached, in particular in material stability and cost, as well as optimization of optoelectronic and electrochemical properties of device components.[1,5–8]

One key challenge for successful PEC lies in identifying a solar absorber material that exhibits an appreciably wide band gap, has an optimized electronic structure at the electrode/electrolyte interface, is stable under normal operating conditions over the lifetime of the device, and can be manufactured at acceptable costs. Chalcopyrites, such as $Cu(In,Ga)(S,Se)_2$ (CIGSSe), are regarded as one of the most prominent absorber materials for use in highly efficient solar devices, as shown by their high photovoltaic conversion efficiencies, both as small cells and as large-area modules.[9] Their variability in composition allows for a tuning of their band gap, and their high absorption coefficient allows for a cost-efficient thin-film fabrication.[8,10] However, for PEC, additional requirements exist – in particular, the band edges need to be optimally aligned with the redox potentials necessary for evolving hydrogen and oxygen gas. A detailed understanding of this alignment and experimentally derived band edge positions are needed for further advancements.

In this paper, a variety of chalcopyrite-based thin-film absorbers with the potential for use as a photoanode material in solar water splitting is presented. Most of them were produced with a focus on photovoltaic applications, including the desire to develop wide-gap materials for utilization in tandem devices. The band edge energies at the surface determined under vacuum conditions can be visualized on an electrochemical energy scale relevant to PEC devices (i.e., relative to the normal hydrogen electrode (NHE)) with the help of the work function determined in the same experiments. With some suitable assumptions, this allows for a direct comparison with respect to the redox potentials for water splitting, across a multitude of chalcopyrite variants, and offers immediate insights in terms of necessary developments for use in PEC and large-scale solar hydrogen production.

The PEC community customarily determines the VBM for p-type systems and the CBM for n-type systems by electrochemical analysis, through "*flatband"* measurements involving standalone electrodes.[11] This type of electrochemical measurement requires specific assumptions regarding flatband conditions, in particular that an electrochemical potential can be applied that removes the band bending in the absorber material, essentially compensating the built-in electrostatic field induced by the surface itself. The complementary band edges, i.e., the CBM for p-type systems and the VBM for n-type systems, are generally extrapolated from this data using bulk band gap values derived optically, most commonly with UV-Vis spectroscopy and a Tauc plot analysis.[12] However, for chalcopyrite materials, it is quite common that the band gap in the bulk differs significantly from that found at the surface .[13–16] In particular, surface band gaps of chalcopyrite absorbers of high-efficiency solar cells are generally appreciably larger than the corresponding optically-derived bulk values due to a modified chemical structure at the absorber surface (generally a reduction in Cu surface content). While this fact points out a shortcoming in

the current electrochemical characterization approach, it also opens up a new optimization pathway: the optical *bulk* band gap is responsible for the absorption of solar photons, while the *surface* of the absorber forms the interface with the electrolyte at which the electrochemical processes are occurring. If the electronic surface band gap can be tailored separately from that of the bulk, then this allows for a much more expansive optimization of the electrochemical activity. For a correct description of the interface energetics, it is therefore necessary to directly determine the band edge positions and electronic band gaps *at the surface*, which can be done using x-ray and UV photoelectron spectroscopy (XPS and UPS) in combination with inverse photoemission spectroscopy (IPES).[17–19]

Before presenting the experimental data, we will discuss the role of the surface band edges in relation to the electrochemical performance of the material. For this purpose, Fig. 1 (a) shows a schematic representation of the relevant energy levels in a PEC device involving a (flat band) n-type semiconductor. Solar photons (not shown) excite electrons inside the semiconductor (left), creating conduction band electrons and valence band holes. Electrons diffuse to the metal back contact and relax to the Fermi level; in the absence of a bias voltage, this is at the same energy as the Fermi level (dashed line, $E_F$) of the counter electrode (right). The center shows the redox potentials involved in water splitting, shifted to represent the assumed need of an overpotential. As can be seen from the plot, the Fermi level needs to lie above the $H^+/H_2$ hydrogen reduction potential to allow for spontaneous water splitting. Likewise, holes need to be transferred to the $H_2O/O_2$ water oxidation level from the VBM.

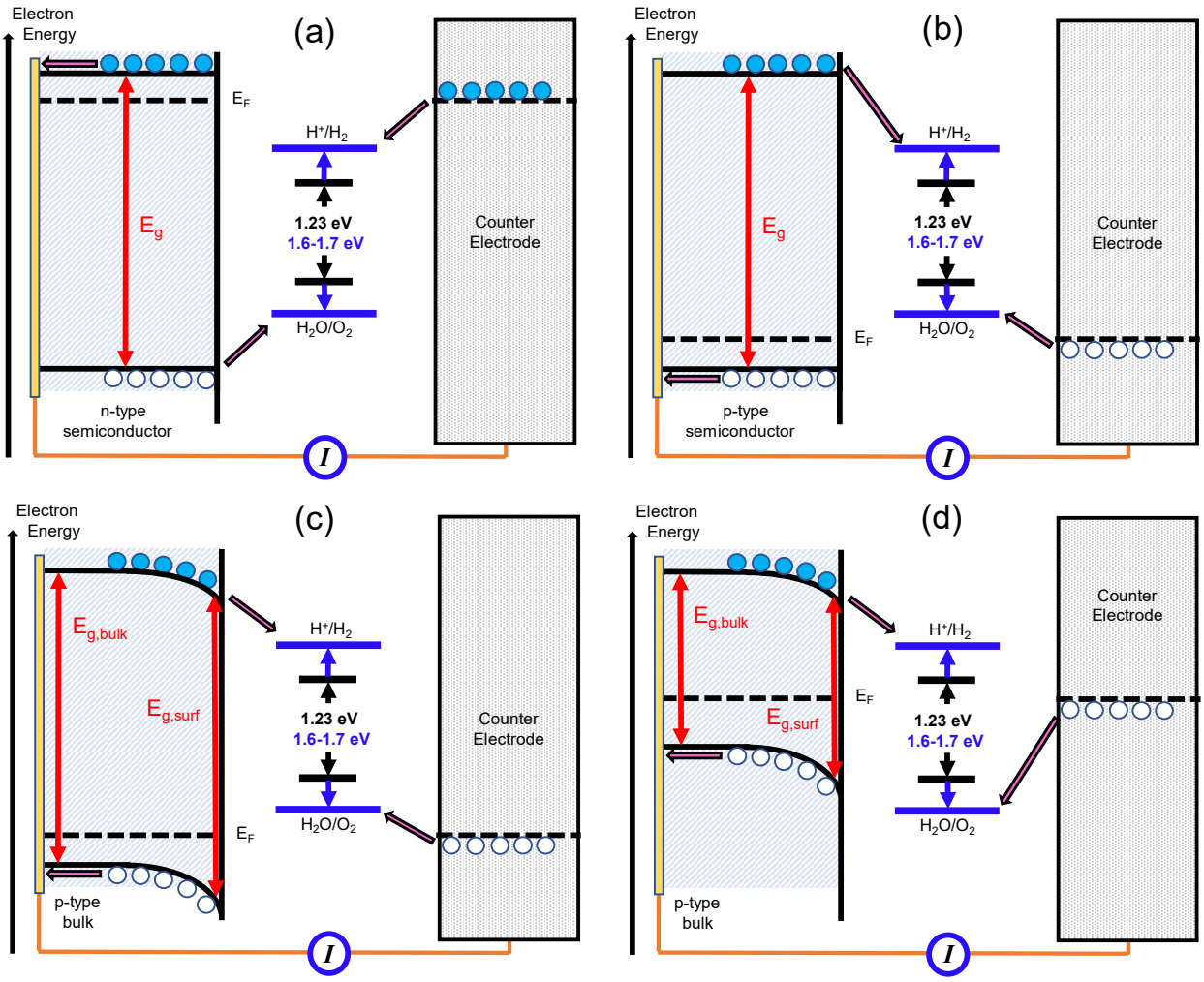


Fig. 1. Schematic representation of a PEC device, consisting of a semiconductor absorber with a metal back contact (left), a metal counter electrode (right), and an electrolyte environment (center). This figure is based on a depiction by John Turner, National Renewable Energy Lab, NREL, but a large variety of similar depictions is found in the PEC literature; a particularly insightful example is Ref.[20] by Nozik & Memming. The abscissa denotes the spatial separation of these three components, while the ordinate represents the involved electron energies and electrochemical potentials. The levels in the electrolyte region depict the redox potentials for water splitting, including an assumed overpotential (increasing the required energy from 1.23 eV, black, to 1.6-1.7 eV, blue arrows and levels). (a): flat-band n-type semiconductor, (b): flat-band p-type semiconductor, (c): wide-gap p-type chalcopyrite absorber with band bending and band gap widening towards the surface, and (d): as (c), but for a narrow-gap absorber. The red "X" in (d) indicates a blocked pathway for holes to reach the water oxidation potential.

As a necessary condition, thus, the band edge positions need to straddle the redox potentials for water splitting: the CBM needs to be above that of the hydrogen reduction potential, while the

VBM has to be sufficiently below that of the water oxidation potential. As a sufficient condition (for an n-type semiconductor with a metal counter electrode), it is actually the *Fermi energy* that needs to lie above the $H^+/H_2$ hydrogen reduction potential. These requirements are all met in the schematic diagram in Fig. 1 (a). Fig. 1 (b) shows the same schematic representation, but now for a p-type (flatband) device. Note that the current now flows in the opposite direction, but that most of the energetic considerations discussed above still hold true: as a necessary condition, the band edges of the semiconductor need to straddle the redox potentials for water splitting. The sufficient condition is now "reversed": the Fermi energy must now lie *below* the water oxidation potential. As will be discussed below, the sufficient conditions can hardly ever be met without an additional bias voltage, because they require surfaces with very large or very small work functions (for n- and p-type surfaces, respectively).

We would like to point out that a refinement of the "sufficient condition" can be considered, namely the splitting of the Fermi level into "quasi Fermi levels" of electrons and holes.[21] This approach becomes applicable when the system is disturbed, not just by one photon (as in our case), but by a large number of photons (e.g., under solar irradiation) or the application of a bias.

However, a number of implicit assumptions, in particular the ability to reach independent equilibria for electrons and holes, respectively, as well as the presence (or, rather, absence) of an Ohmic contact makes this approach questionable, suggesting that a band-edge description is still a better model. Since the splitting of the quasi Fermi levels furthermore depends on the intensity of the disturbance (i.e., the photon flux or the magnitude of the bias) and such internal parameters as the material's recombination rate (e.g., in $Cu(In,Ga)Se_2$ thin-film PV material),[22] we have refrained from applying this concept here.

For a true *chalcopyrite* solar device, the energy level depictions in Figs. 1 (a) and (b) need to be further refined, as sketched in Fig. 1 (c). In the bulk, chalcopyrite materials are generally considered to be p-type,[23,24] with a significant downward band bending towards the surface that allows for efficient charge carrier separation. Chalcopyrite surfaces are thus sometimes incorrectly called "n-type". Furthermore, as mentioned above, it is now commonly accepted that the absorbers of highly efficient devices have a different composition at the surface than in the bulk, in particular a reduction of the Cu content at the surface; this leads to a band gap widening at the surface.[13–16] These features are all incorporated in Fig. 1 (c). As is evident from Fig. 1 (c), the (bulk) band gap of the chalcopyrite layer needs to be rather wide for the band edges to straddle the redox potentials for water splitting (as a necessary condition) and the Fermi energy to lie *below* the water oxidation potential (sufficient condition).

Furthermore, a semiconductor with a built-in band bending, such as the one depicted in Figs. 1 (c), will provide an internal bias voltage between its surface and its back contact when illuminated with sufficiently intense solar irradiation. Such voltages can potentially be as high as the open-circuit voltage of a corresponding photovoltaic device.

None of the compositions for chalcopyrite absorbers generally used in PV cells possess wide band gaps and large work functions, but many promising pathways exist, including the increase of Ga and/or S content and the alloying with additional elements that promise wider band gaps, up to 2.43 eV.[10] Furthermore, individual cells could be stacked (e.g., in a tandem configuration) or an external bias could be applied to achieve a higher energy separation between the Fermi level of the counter electrode and the CBM at the semiconductor surface. In fact, many efforts in the CIGSSe PEC community are focused on tailoring the optical properties for a tandem configuration, rather than their surface energetics, which will have to be adjusted with buffers.[25]

This paper presents chalcopyrite materials that either were optimized for PV applications or represent a first step in the development of wide-gap chalcopyrite materials specifically dedicated to PEC. To illustrate the challenges that lie ahead, Fig. 1 (d) gives a (short-circuit) representation of a chalcopyrite PEC device that will *not* spontaneously split water (see the path blocked by the red "X"). Even under solar irradiation in an open-circuit scenario, this device would not be able to produce sufficient bias. Nevertheless, Fig. 1(d) best represents most of the experimental results obtained in this study - the Fermi level clearly lies above the water oxidation potential.

Note that the electronic structure of a CIGSSe device towards the (commonly employed) Mo back contact is also significantly more complex than described in the figures. For a detailed description see, e.g., Refs.[26–29]. However, this back-contact structure is optimized to facilitate charge carrier transport across the back interface and will hence not be further considered here.

To now obtain data and develop descriptions that can be compared to the models in Fig. 1, several experimental data points need to be collected. First of all, the surface VBM needs to be determined with respect to the Fermi energy, which can be readily achieved by a UPS measurement of the relevant surface. Likewise, IPES can be employed to determine the surface CBM with respect to the Fermi energy. Combining VBM and CBM also allows for a determination of the electronic surface band gap, as well as the position of the Fermi level within the gap (a unique information not attainable by any other spectroscopic approach). To complement the data set, the work function of the surface needs to be determined, to describe the electronic surface structure relative to the vacuum level.

## METHODS

In this paper, CIGSSe samples of various composition and fabrication are analyzed and evaluated on three different energy scales, namely with respect to the Fermi energy, with respect to the vacuum level, and with respect to the NHE scale, pertinent to that of a complete PEC device. For this purpose, previously published and unpublished data is being combined to paint a comprehensive picture of the variations in surface electronic structure that are induced by different preparation processes and surface compositions. To properly classify the surface chemical compositions, the following abbreviations will be used: CISe [i.e., $CuInSe_2$, without Ga and S at the surface], CISSe [i.e., $CuIn(S,Se)_2$, without Ga, but with S at the surface], CIGSe [i.e., $Cu(In,Ga)Se_2$, with Ga, but without S at the surface], CIGSSe [similarly], and CIGS [similarly].

The CISe sample, previously studied in Ref. [14], was taken from the Siemens & Shell Solar baseline process,[30] involving rapid thermal annealing/processing (RTP) of elemental layers onto Mo-coated soda-lime glass. The CISe absorber does contain Ga in the bulk, but only trace amounts were found near the surface – a common finding for absorbers prepared by the RTP process. The CISSe sample, previously studied in Ref.[15], was also taken from the Siemens & Shell Solar base line process (i.e., prepared by RTP of elemental layers on Mo-coated soda-lime glass); it also included annealing in a *sulfur-containing atmosphere*. The bulk of the CISSe absorber again contains Ga, but the Ga content at the surface is negligible.

The CIGSe absorber in this study was prepared by the Zentrum für Sonnenenergie- and Wasserstoff-Forschung Baden-Württemberg (ZSW), Germany, using co-evaporation of Cu, In, Ga, and Se onto a Mo back contact.[31,32] A second ZSW CIGSe absorber, again prepared by co-evaporation of Cu, In, Ga, and Se onto a Mo back contact, was further treated with a rubidium fluoride post-deposition treatment (RbF-PDT).[33–35]

The CIGSSe surface of this study was produced by AVANCIS GmbH, Germany, using a process variation that also builds Ga into the surface.[36]

For the "pure sulfide" absorbers, the first complete electronic and chemical surface structure representation was given in Refs.[37,38]. The samples were prepared by the Florida Solar Energy Center (FSEC, Dr. Neelkanth Dhere et al.) in a two-stage process. In the first step, Cu, Ga, and In layers were sputter-deposited onto Mo-coated stainless steel foils. In the second step, the metal alloy was sulfurized by rapid annealing in an $H_2S$ atmosphere. Afterwards, the sample surfaces were etched in KCN solution,[39] leaving a K-containing residue on the surface.[38]

The last samples to be assessed were grown by the Hawaii Natural Energy Institute (HNEI), combining the "pure sulfide" approach with Ga alloying and careful KCN etching. Metal alloy precursors were prepared using a two-stage vapor deposition. First, Cu, In, and Ga metal were evaporated from metal sources onto a Mo-coated soda-lime glass substrate. During the second stage, only Cu was evaporated, creating a Cu-rich surface. The CuInGa (CIG) metal alloy, briefly exposed to air, was transferred to a sulfurization chamber and exposed to a sulfur-containing atmosphere at 600° C for 30 minutes, followed by KCN etching.[40]

Unless otherwise noted in the cited original publications, samples were briefly exposed to air after growth, packaged, and vacuum-sealed before being sent to UNLV. There, samples were unsealed in a $N_2$-filled glovebox, mounted, and placed into the UHV system (base pressure $< 5 \times 10^{-10}$ mbar) without any further air exposure. XPS (Mg and Al $K_\alpha$) and UPS (He I and II) measurements were performed using a SPECS PHOIBOS 150 electron analyzer with a delay-line detector. XPS spectra were calibrated using core-level peaks of sputter-cleaned Au, Ag, and Cu foils.[41] UPS and IPES spectra were calibrated using the Fermi energy of the Au foil. IPES spectra were collected using a Staib NEK-150 low-energy electron gun, coupled to a custom-built Dose-

type detector filled with an $I_2$:Ar gas mixture. Note that UPS and IPES measurements involve electrons of kinetic energies between 7 and 41 eV. In this energy range, typical inelastic mean free paths lie in the range of a few nanometers, corresponding to the length after which a monochromatic beam of electrons is exponentially reduced to 1/e of its original intensity.[41] Hence, the electronic surface structure determined here primarily stems from the first ~5 nm of the surface, integrated over an exponentially decaying distribution function.

## ENERGY LEVEL CONSIDERATIONS

To use the derived VBM and CBM for insights into the operation of corresponding PEC devices, their values must be analyzed relative to the redox potentials for water splitting. While the measured energies are obtained relative to the Fermi level ($E_F$), their values can be related to the redox potentials by combining the experimental work function and the absolute potential of the NHE. Per recommendations provided by the International Union of Pure and Applied Chemistry,[42] the following expression is used to align the energy scales relative to the NHE and the vacuum level ($E_{Vac}$), respectively:

$$-E(\mathrm{NHE}) - 4.44\ \mathrm{eV} \pm 0.02\ \mathrm{eV} = E_{vac} = E_{Fermi} + \Phi, \qquad \text{Eq 1}$$

where $\Phi$ is the work function of the sample surface and -4.44 eV is the absolute potential of the NHE. A difference of 4.44 eV between the NHE and vacuum level scales also gives a lower (n-type surface) or upper (p-type surface) bound for the work function of the surface under study to fulfill the "sufficient" condition in each case - even for the minimal energy required for water splitting (1.23 eV, no overpotential) and assuming a metal counter electrode, these work functions amount to 5.67 and 4.44 eV, respectively. In our case of a p-type chalcopyrite bulk with a downward band bending towards the surface, the former number is relevant. While we have

observed chalcopyrite work functions as high as 5.2 eV[43], work functions around 5.7 eV are generally only found for select surfaces of some of the noble metals. Some metal oxide surfaces can also potentially exhibit work functions in this range (see, e.g., Ref [44], but note again that the work function is not a materials property, but rather a surface property). Nevertheless, in the general case (and if an overpotential is needed), a bias voltage will be required to fulfill the "sufficient" condition. Consequently, a primary goal of chalcopyrite materials (surface) development must be to minimize the necessary bias.

To correlate the vacuum-based measurements with an electrochemical energy scale, two further notable aspects have to be considered. First, one could ask whether the energetics of the absorber surface will change in the presence of an electrolyte, i.e., whether there are differences in absorber surface band bending between the absorber/vacuum interface versus the absorber/electrolyte interface. The latter interface involves an additional element of complexity due to the presence of an electrical (Helmholtz) double layer (EDL).[45] A second consideration must be given to the effects of changing the pH, as the hydrogen evolution reaction (HER) and the oxygen evolution reaction (OER) potentials are typically reported for pH = 0. pH = 0 corresponds to the $[H^+]$ concentration first adopted for the standard and normal hydrogen electrodes (SHE and NHE, respectively); they only differ in assuming ideality of the involved solution. Thus, an experiment at a pH value different than zero will require a correction of the NHE energy scale; for oxides, this is found to be approximately 60 meV per unit of pH.[46] Since the desired pH value for a given chalcopyrite PEC cell is *a priori* not known, we will represent all energy diagrams under the assumption of pH = 0 for connecting the NHE scale and the vacuum level scale. A *complete* description then would either require the "equivalent pH value" of our UHV measurements (which

is neither known nor controlled) or, conversely, a similar experiment in electrolyte and *operando* conditions (such experiments are currently in preparation).

Regarding the first consideration, it has indeed been previously reported that the band bending at a solid/vacuum interface can differ from that of a solid/electrolyte interface.[17] This is due to the formation of the EDL, which can be described as an array of oriented dipoles at the solid/electrolyte interface.[45] The space between the adsorbed ions and those ions closest in solution is called the inner Helmholtz layer.[45] Just as the surface of a semiconductor will exhibit a surface dipole when in vacuum, a dipole can also manifest at the surface in the presence of an electrolyte, causing an additional band bending at the interface due to electrostatic interactions between the electrolyte and the absorber surface.[14,47,48]

The Helmholtz double layer and its dipolar interaction with the absorber surface, thus, do not fundamentally differ from the changes induced by a modification of the surface dipole, e.g., by adsorbates, modifications of surface state occupancy, or other dipole modifications. It will thus depend on the specific characteristic of the absorber surface whether this dipole modification will lead to additional band bending. If the Fermi level at the surface is "pinned", e.g., if a sufficient number of surface states exists that can accommodate additional charges, and/or if the surface dipole is not substantially modified by the EDL formation, then no significant additional band bending needs to be taken into account.

In the case of chalcopyrite absorbers, such additional band bending is expected to be rather small, based on the experimentally observed additional band bending in the absorber induced by interface formation with various buffer layers in photovoltaic devices (including CdS and Zn(O,S)). In all of these cases, interface-induced band bending changes in the absorber are

typically on the order of 0.1 eV or less (see, e.g., Refs.[15,49,50]), and hence this aspect will not be further considered here.

## RESULTS AND DISCUSSION

For an all-experimental description of the electronic structure of PEC candidate materials, we now follow the approach described in Refs. [51–53] First, we collect He II UPS and IPES spectra of the valence band and conduction band region, respectively. A linear extrapolation of the leading edge is employed to determine the VBM and CBM. For the suitability of this approach, see Refs. [54,55]. From the He I-excited UPS spectrum, we furthermore determine the secondary electron (SE) cut-off to derive the work function. These energies are then given with respect to the Fermi energy of the experimental system, as determined with a reference Au foil; this allows the depiction of all three spectra on the same energy scale. An example of this is shown in Fig. 2 (left), which shows the valence and conduction bands, as well as the SE cut-off, for a CISe thin-film surface. The UPS and IPES data was taken from Morkel et al.,[14] while the work function measurement is taken from Ref.[56] Below Fig. 2 (a), a schematic representation of the experimental results for this CISe absorber surface is shown, including the VBM, CBM, and VL energies with respect to the Fermi level.

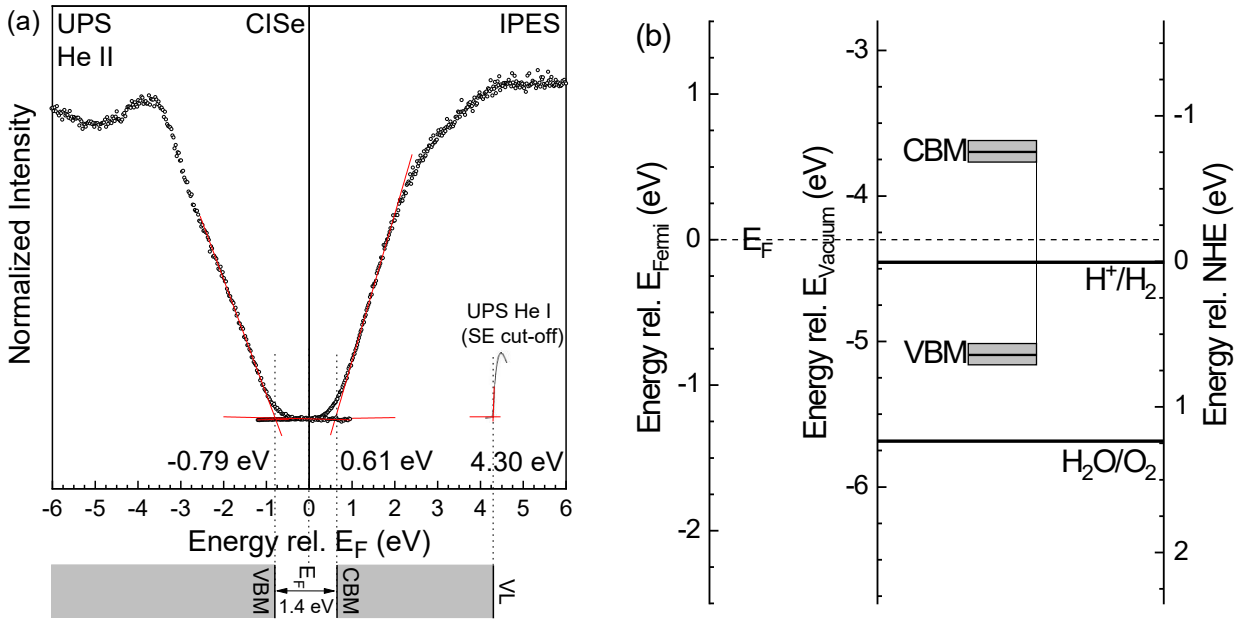


**Figure 2 (a)** UPS (left) and IPES (right) spectra of a **$CuInSe_2$ (CISe)** Siemens & Shell Solar (now AVANCIS) absorber surface, as measured by Morkel et al. in 2001.[14,56] The VBM and CBM were determined by linear extrapolation of the leading edges after a total of 14 min of 500 eV $Ar^+$ ion sputtering treatments. The electronic band gap at the surface was found to be 1.4 (± 0.15) eV. The secondary electron cutoff, as measured by UPS, is shown in the lower right corner. A work function of 4.30 (± 0.05) eV was derived by linear extrapolation.[56] Below the graph, a schematic representation of the band edges and the vacuum level (VL) is given. **(b)** VBM and CBM of the **CISe** absorber surface, depicted relative to the Fermi energy, the vacuum level, and the normal hydrogen electrode (NHE). Confidence regions for the VBM and CBM are shown in gray. The water oxidation and hydrogen reduction potentials are drawn for comparison.

The Morkel measurements gave first *direct* evidence for a widened band gap at the surface of high-efficiency chalcopyrite absorber films, as postulated by Schmid et al.[13] The expected optical bulk band gap for a CISe surface is 1.04 eV,[57] while Morkel's study found a surface band gap of 1.4 eV, as shown in Fig. 2 (left). The VBM was found ~0.8 eV below the Fermi energy, while the CBM was found ~0.6 eV above $E_F$. The work function was determined to be 4.30 eV.

To now gain insights into the potential utilization as a PEC material, Fig. 2 (b) shows the results with different reference energies, i.e., relative to the vacuum level and the NHE. First, we employ the experimental work function to shift from an energy scale relative to the Fermi level ["Energy rel. $E_F$ (eV)"] to one relative to the vacuum level ["Energy rel. $E_{Vacuum}$ (eV)"].

Next, we use Eq. 1 to relate the vacuum level to the NHE, following the IUPAC recommendation discussed previously. After doing this, we can depict the band edge positions in relation to the redox potentials for water splitting at normal conditions. In the case of the AVANCIS CISe surface, the CBM lies 0.73 eV above the $H^+/H_2$ reduction potential, while the surface VBM lies 0.59 eV *above* the $H_2O/O_2$ oxidation potential, as shown in Fig. 2 (right). Furthermore, the Fermi level of the cathode is higher than that of the $H^+/H_2$ reduction potential.

This surface is hence best described by the schematic representation in Fig. 1 (d), and the overall configuration will not be suitable as a PEC device (by itself). This is not surprising, as the observed band gap, even if it is wider than expected from the nominal composition and optical bulk band gap measurements, is too narrow for providing the necessary potential difference for water splitting *plus* the required overpotential to drive the reaction. Consequently, CIGSSe absorbers with wider band gaps are required to straddle the redox potentials for spontaneous water splitting.

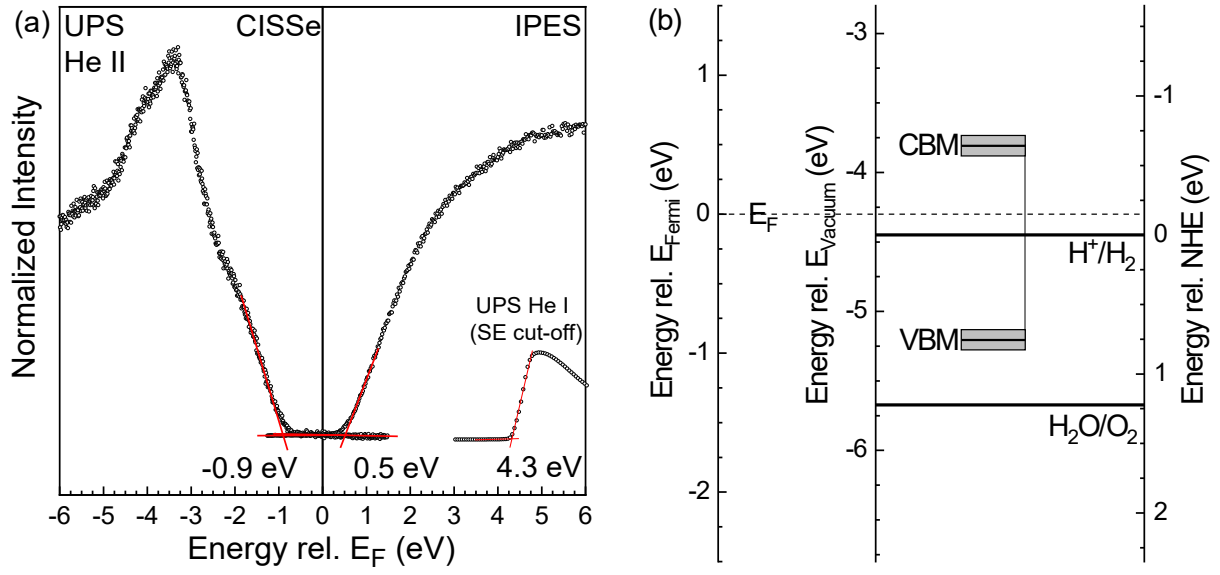


**Figure 3 (a)** UPS (left) and IPES (right) spectra of a Siemens & Shell Solar (now AVANCIS) CISSe absorber surface, as measured by Weinhardt et al. in 2001.[15] The SE cutoff (bottom right) is also given.[58] Linear extrapolations of the leading edges are shown to determine the VBM, CBM,

and work function (vacuum level) values (depicted schematically below the graph). **(b)** PEC plot of the CISSe sample surface, based on the data presented on the left.

One possibility to modify the band gap is to incorporate S into the chalcopyrite lattice, which is expected to increase the (bulk) band gap up to 1.54 eV, depending on the S/(S+Se) ratio (SSSe ratio).[10] A priori, it is not directly evident whether the (indeed observed) increase in bulk band gap will also translate into a (further) increased surface band gap. In fact, as found by Weinhardt et al. in 2001,[15] this is not the case for the Siemens & Shell Solar CISSe absorber surface: the UPS and IPES data shown in Fig. 3 (a) clearly indicate an electronic surface band gap of 1.4 eV, as in the S-free case. Furthermore, the same work function (4.3 eV) was found,[58] and hence the PEC plot for CISSe (Fig. 3 (b)) is very similar to the one of CISe in Fig. 2, with a small downward shift of 0.1 eV of the VBM and the CBM (w.r.t. $E_F$, VL, and NHE).

As in the case of the CISe absorber in Fig. 2, the PEC plot does not depict a device suitable for spontaneous water splitting. Again, this is not necessarily surprising, as this particular absorber surface was optimized for high-efficiency thin-film PV modules (with current record efficiencies up to 19.6 % for modules with an aperture area of 671 $cm^2$).[59]

Independent from the variation of the SSSe ratio, the band gap of chalcopyrites can be increased by the addition of Ga, and further modified with the Ga/(Ga+In) (GGI) ratio. In fact, one of the secrets of the chalcopyrite's success in thin-film PV is a meticulous optimization of the GGI ratio throughout the depth of the absorber.[24,60] For a pure CGSe, an optical bulk band gap of 1.68 eV is reported (Ref.[10] and references therein). Best PV efficiencies are generally reported for a GGI ratio near 0.3.

Fig. 4 depicts the electronic surface structure of a CIGSe absorber, prepared by the ZSW.[31,32] The ZSW, up until recently,[61] held the world-record in CIGSSe PV efficiency by

introducing a RbF post-deposition treatment (RbF PDT). The data shown in Fig. 4 was taken for the (sulfur-free) CIGSe absorber surface, world-record grade, both before and after the RbF PDT treatment.[33,35]

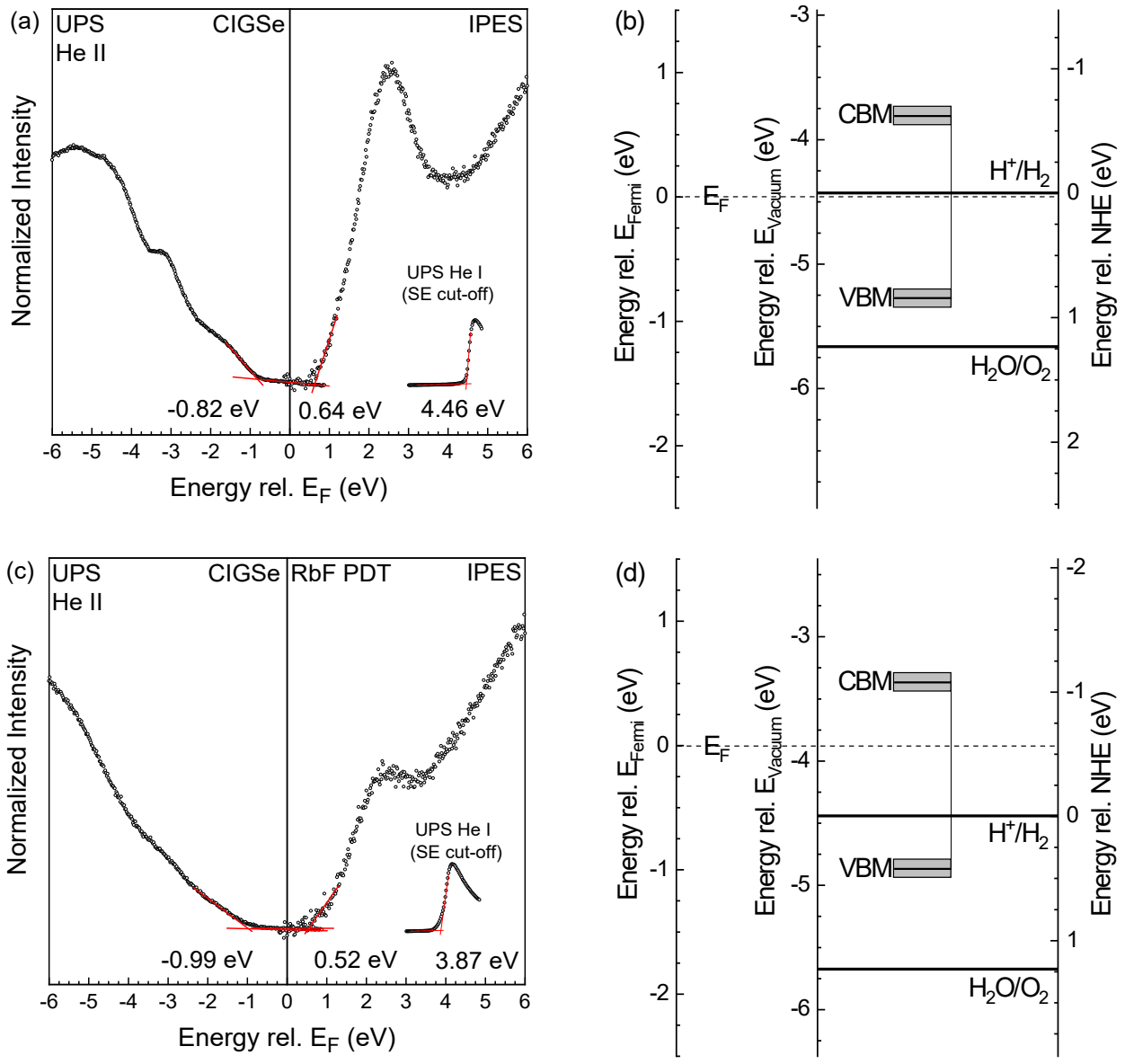


**Figure 4** UPS and IPES spectra of the ZSW CIGSe absorber surface before (a, top) and after (c, bottom) a RbF PDT as measured by Hauschild et al. in 2017.[33] The secondary electron cutoffs (bottom right) are also given. (b) and (d): corresponding PEC plots.

As can be seen in Fig. 4 (a), the inclusion of Ga does indeed widen the band gap at the absorber surface – a surface band gap of 1.46 (± 0.11) eV is found; the surface VBM is determined to be 0.82 eV below the Fermi energy, while the CBM lies 0.64 eV above $E_F$. With a work function of 4.46 eV, the transfer to the vacuum level and NHE energy scales yields a Fermi energy that

essentially coincides with the $H^+/H_2$ reduction potential, as shown in Fig. 4 (b). The surface VBM lies 0.30 eV above the $H_2O/O_2$ oxidation potential, which is roughly 0.3 eV less than for the CISe absorber surface described in Fig. 2. While this would also not enable spontaneous water splitting, it nevertheless suggests that Ga surface inclusion might be a more promising pathway than the alloying with sulfur (shown in Fig. 3).

After RbF-PDT, the electronic levels change, as illustrated in Fig. 4 (c) and (d). While the electronic surface band gap is not significantly affected (difference of 0.05 eV), two main effects are found.[33,35] First, compared to the absorber without RbF-PDT, the band edges are shifted downwards by ~0.1 eV. In Ref. [33], it is furthermore reported that they additionally shift downward upon interface formation with a CdS buffer, suggesting a passivation of surface defects that would otherwise pin the Fermi level at the values found for the solid/vacuum interface. Secondly, the detection of residual Rb on the surface explains the observed substantial reduction of the work function, from 4.46 eV to 3.87 eV. This is a common finding for alkali-covered surfaces,[62] and has significant impact for the PEC plot in Fig. 4 (d). We note, however, that a surface decoration with alkali-containing compounds will likely not be stable at the solid/electrolyte interface. While the interaction between alkali atoms and water on a CIGSSe surface is very complex,[63] one of the main effects is a removal of the alkali atoms into the solution environment. Nevertheless, it is instructive to investigate the impact on the PEC plot in detail, as given in Fig. 4 (d). Now, the surface CBM lies 1.1 eV above the $H^+/H_2$ reduction potential, while the surface VBM lies 0.71 eV above the $H_2O/O_2$ oxidation potential. Due to the significant difference in work function, the VB edge is shifted further away from the water oxidation potential, and the Fermi level is found significantly above the $H^+/H_2$ reduction potential.

The observed effect also suggests a new pathway for potential optimization of chalcopyrite surfaces for PEC, and furthermore gives a new point of view for the conceptual visualization of how surface properties (or properties at the solid/vacuum interface) transition to properties at the solid/*electrolyte* interface. While chalcopyrite surfaces typically exhibit work functions in the range of 4.0-4.5 eV (as in the cases discussed so far), a combination of ion-sputter/annealing cycles can lead to work functions above 5 eV.[43] Conversely, separate alkali or water adsorption (in UHV) lead to a reduction in work function, while co-adsorbed water molecules can, in turn, diminish the magnitude of the alkali-induced work function reduction.[63] This shows the unique nature of water molecules (and hence the Helmholtz double layer) to accommodate and alter the orientation of their dipoles to the electrostatic environment at surfaces and interfaces.

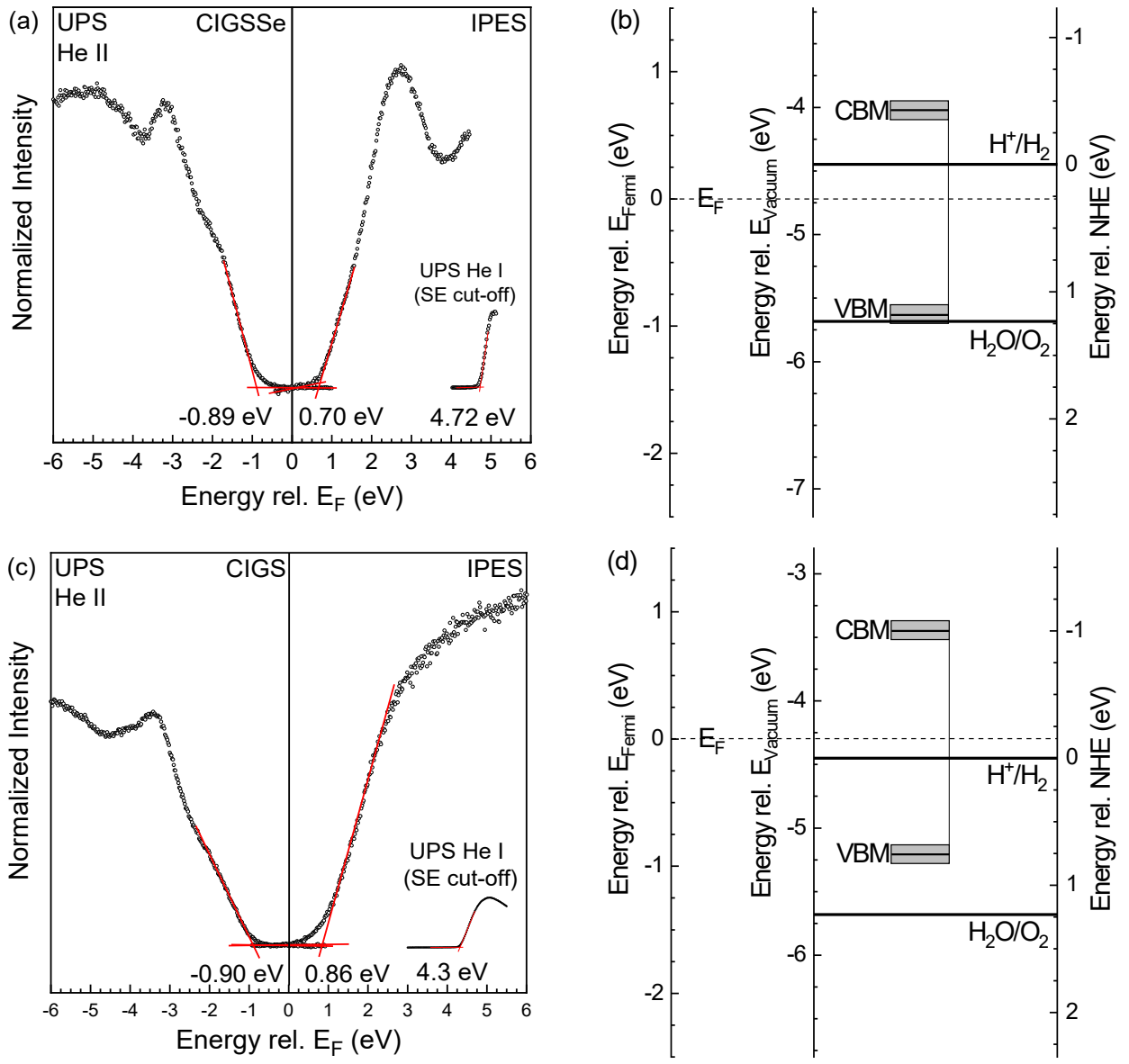


**Figure 5** (a) AVANCIS CIGSSe absorber surface, and (c) CIGS absorber surface manufactured by the Florida Solar Energy Center (FSEC):[37] UPS, IPES, secondary electron cutoff; (b) and (d): corresponding PEC plots.

In Fig. 5 (a), we now focus on a novel CIGSSe surface from AVANCIS, i.e., in which both S *and* Ga are incorporated at the surface. Caused by the S- and Ga-alloying, together with the formation of a Cu-poor surface region, the observed electronic surface band gap is, indeed, wider than any of the surface band gaps discussed so far. With a VBM at -0.89 eV and a CBM at 0.70

eV, a surface band gap of 1.59 (± 0.11) eV is derived. With a relatively large work function (4.72 eV), the Fermi energy is now found between the water splitting redox potentials, and they, in turn, are almost straddled by the band edges, with the VBM only 0.06 eV above the $H_2O/O_2$ oxidation potential and the CBM 0.43 eV above the $H^+/H_2$ reduction potential. While this is close to fulfilling the above-mentioned necessary conditions, this surface will also not work for spontaneous water splitting, since the Fermi level is still ~1 eV *above* the $H_2O/O_2$ oxidation potential (sufficient condition).

Nevertheless, this example does outline a promising strategy towards optimizing chalcopyrite materials for solar water splitting, namely to combine various approaches to (a) increase the bulk/surface bands gap of the material (such as alloying with S and Ga, but maybe also other elements such as Al,[64] Ag,[65] or B[66]), and (b) modify the surface to achieve a large(r) work function. In approach (a), it even appears possible to *combine* different alloying approaches (i.e., simultaneous S and Ga alloying) for favorable results**.**

We now turn to "pure sulfide" absorbers. The spectra, their analysis, and the corresponding PEC plot are also shown in Fig. 5 (c and d). As for some of the alkali-covered examples shown and discussed above, the work function of this surface is relatively small (4.3 eV), and hence the CBM and VBM positions are also relatively "high" in the PEC plot (the CBM lies 0.99 eV above the $H^+/H_2$ reduction potential, and the VBM is found 0.47 eV *above* the $H_2O/O_2$ oxidation potential). Compared to all previous systems, this surface exhibits the widest band gap so far (1.76 eV), indicating that the "pure sulfide" system might be particularly suitable for PEC applications. Nevertheless, the work function will need to be monitored and optimized. In the here-described context of a PEC device, the work function must be maximized, which might be in direct

competition with the effects of residual K from KCN etching after absorber growth (generally required to remove detrimental copper sulfide phases from the surface of S-only absorbers).[38,39]

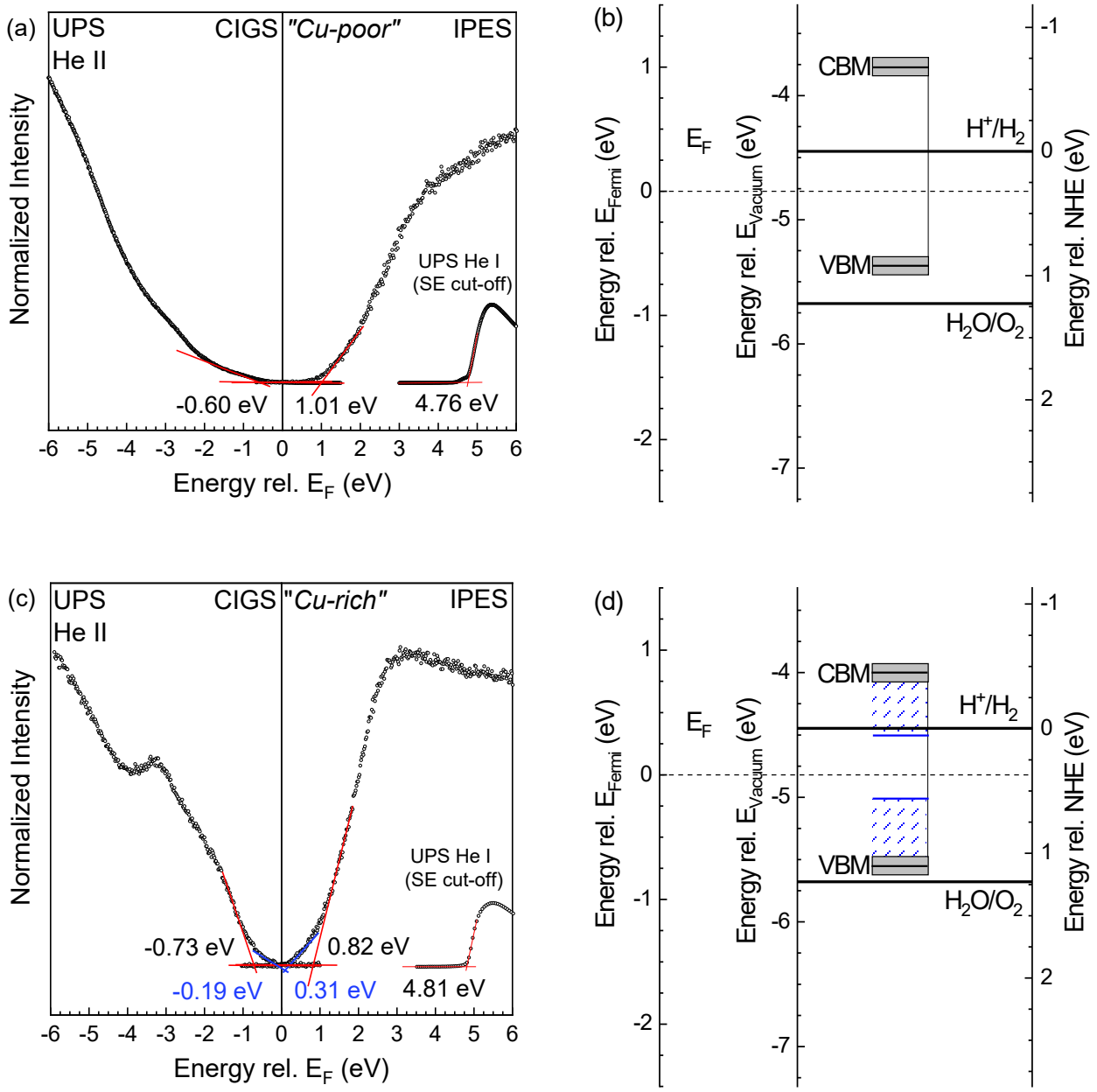


**Figure 6** HNEI CIGS "copper-poor" (a) and "copper-rich(er)" (c) absorber surfaces: UPS, IPES, secondary electron cutoff; (b) and (d): corresponding PEC plots.

These observations now lead us to two novel custom-tailored solar absorbers, intended as a first optimization step towards using chalcopyrites for PEC applications (Fig. 6). Grown by HNEI, these surfaces combine the "pure sulfide" approach with Ga alloying and careful KCN etching.

Both sample surfaces are Cu-poor compared to the nominal bulk composition of 1 : 1 : 2 for Cu : (In+Ga) : (S+Se), with approximate stoichiometries of 1 : 3 : 5 (in the following denoted "Cu-poor") and 1 : 2 : 4 (i.e., with a higher Cu concentration than the first sample, hence in the following denoted "Cu-rich"). The surface GGI ratios were determined to be 0.28 ± 0.05 ("Cu-poor") and 0.37 ± 0.05 ("Cu-rich"). The "Cu-poor" surface, with a band gap of 1.61 (± 0.11) eV and a work function of 4.76 eV, agrees well with the previous work on the sulfide-only chalcopyrite system in Fig. 5 (bottom). In contrast, the "Cu-rich" surface (work function of 4.81 eV) exhibits an unusual electronic structure in the UPS and IPES spectra. To demonstrate this, we have included two sets of linear extrapolations (red, VBM = -0.73 eV, CBM = 0.82 eV, and blue, VBM = -0.19 eV, CBM = 0.31 eV). The red linear extrapolations lead to an electronic surface band gap of 1.55 (± 0.11) eV, similar to the gap of the "Cu-poor" surface. However, these linear extrapolations leave substantial spectral tails undescribed (as shown with the blue linear extrapolation in Fig. 6c and blue markings in Fig. 6d, leading to a "band gap" of 0.50 (± 0.11) eV). While such tails are not uncommon in the description of transparent conductive oxides[67,68], they are rather unusual in the case of chalcopyrites. We hypothesize that the seemingly narrow "band gap" can be attributed to a much greater number of surface defects compared to its "Cu-poor" counterpart, as we could not find any evidence suggesting the presence of additional binary phases, unique chemical bonding environments, or even any gradual changes in surface composition.

In both cases, the absence of residual K (and Na) on the surface (not shown) leads to a comparatively large work function (4.76 and 4.81 eV, respectively). However, the electronic structure is not quite as was hoped for based on the earlier "pure sulfide" measurements – the "Cu-poor" surface shows a band gap of (only) 1.61 eV, and the "Cu-rich" surface (band gap of 1.55 eV) furthermore exhibits a substantial amount of surface defects.

Consequently, neither of the two surfaces represents an improvement in the PEC plot. For the sample with the "Cu-poor" surface, Fig. 6 suggests that further improvement can be achieved with a wider band gap (i.e., with a higher GGI ratio, other alloying partners, or, possibly, further Cu depletion), and an enhanced surface band bending, shifting the band edges further downwards. This can possibly be achieved by additional surface engineering (i.e., beyond simple KCN etching and rinsing) to passivate surface defects that otherwise pin the Fermi energy, and by introducing additional charges at the semiconductor surface that lead to an additional downward band bending. The "Cu-rich" sample in Fig. 6 demonstrates that such modifications need to be implemented with great care, as the creation of unwanted surface defects will most likely be detrimental for PEC performance.

The results found for the different samples are summarized in Fig. 7. While the previous PEC plots used the (experimental) Fermi energy scale as the common energy axis, here all sample surfaces are depicted on a common NHE scale. For reference, the CISe sample surface (far left panel) has also been plotted with its $E_F$ and $E_{Vacuum}$ scales.

It is evident from Fig. 7 that all chalcopyrite surfaces analyzed here exhibit a CBM that is well above the $H^+/H_2$ hydrogen redox potential, fulfilling one aspect of the "necessary condition". The VBM, in contrast, generally lies "too high", in some cases well above the water oxidation level. Nevertheless, in some cases (e.g., for the CIGSSe and CIGS surfaces), this difference is only

0.5 eV or less; a further optimization of the SSSe and, in particular, the GGI ratios might lead to a "straddling" situation. None of the Fermi energies lie below the water oxidation level (i.e., the "sufficient condition" for spontaneous water splitting). As discussed earlier, this fact can be remedied by a bias voltage, in part even produced by the solar irradiation itself. In some cases, this bias voltage would have to be very large (e.g., for the CISSe surface), but again the novel CIGSSe and some of the CIGS surfaces suggest that the required bias voltage can be reduced by optimizing the SSSe and GGI ratios (in some cases to less than 1 V). Alloying with other elements that allow for larger band gaps (like aluminum, silver, or boron) promises to be a pathway towards wider band-gap chalcopyrites, possibly further reducing the necessary bias voltage. Finally, we point out that suitable surface modification (possibly even with an additional thin overlayer, for example of a metal oxide) can further optimize the energetics of the PEC system. However, great care must be taken that the surface modification does not lead to an excessive creation of surface defects that can potentially hinder charge transport (as in the case of the CIGS HNEI "Cu-rich" sample).

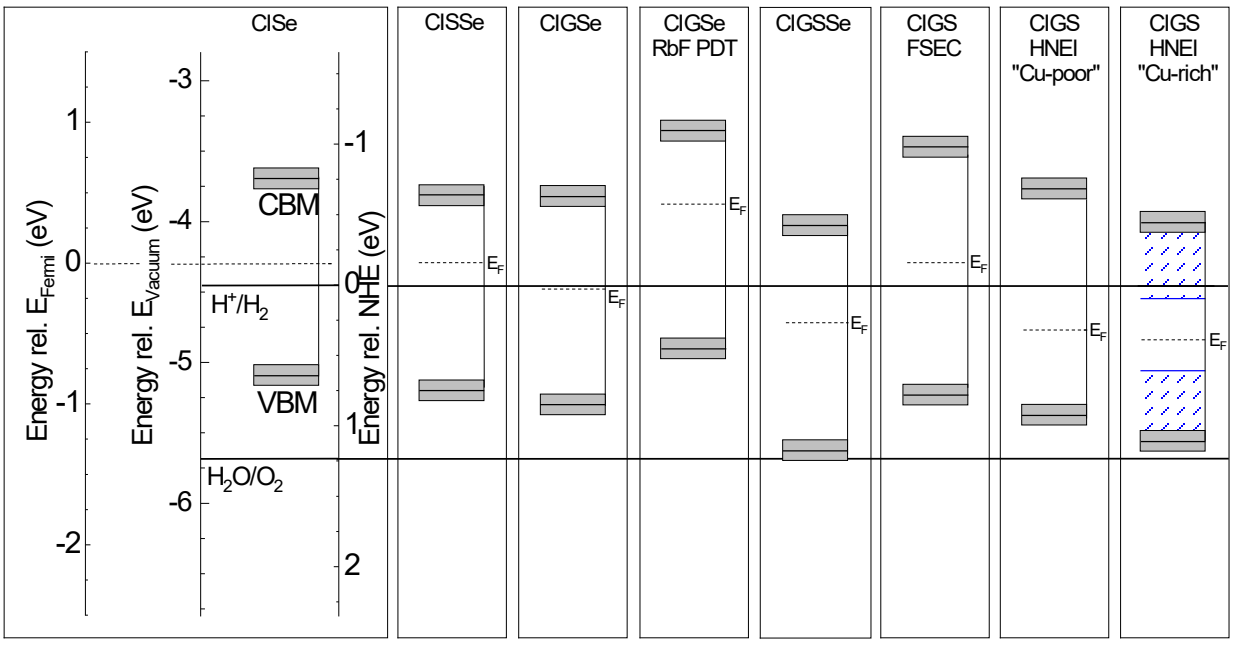


**Figure 7 Far left panel:** Band edges for a CISe absorber, presented on an energy scale relative to

the Fermi Energy ($E_{Fermi}$ or $E_F$), the vacuum level ($E_{Vacuum}$), and the Normal Hydrogen Electrode (NHE). **Other panels:** Derived energy levels for various $Cu(In,Ga)(S,Se)_2$ absorber surfaces with respect to the NHE. The oxidation and reduction potentials for water, as well as the Fermi Energy are also shown for comparison.

## CONCLUSIONS

Experimentally determined energy levels of a variety of chalcopyrite surfaces, derived from vacuum-based electron spectroscopy methods, have been correlated to an electrochemical energy scale pertinent to that of a complete PEC device, highlighting the importance of understanding the band edge positions and band alignment with the reduction-oxidation potentials necessary for solar water splitting. "PEC plots" for various $Cu(In,Ga)(S,Se)_2$ absorber surfaces were presented in an effort to derive guidelines for further optimization of chalcopyrite thin film materials for their use as solar water-splitting materials.

The energy diagrams show a CBM well above the $H^+/H_2$ hydrogen redox potential, while the VBM also generally lie above that of the $H_2O/O_2$ water oxidation potential. As a "necessary condition", straddling band edges need to be achieved by further widening the surface band gap. Several promising pathways (and material candidates) exist, e.g., by further optimizing the Ga/(Ga+In) and S/(S+Se) ratios, as well as by alloying with additional elements.

The energetics of the PEC process likely dictate the need for a bias voltage when using chalcopyrite surfaces. However, surface modification treatments, including the addition of a thin overlayer, will further allow for a variation and optimization of surface electronic structure to minimize required bias voltages. Care needs to be taken to minimize additional surface defects when deliberately modifying the surface chemical and electronic structure in this case. Overall, our study shows that chalcopyrites remain a promising candidate for solar water splitting, given its variability and unique surface properties. However, further studies and material/surface variations need to be conducted to advance towards a commercially viable PEC pathway.

**ACKNOWLEDGMENT**

The work performed by UNLV and HNEI was supported by the U.S. Department of Energy under contract DE-EE0006670 “Wide Bandgap Chalcopyrite Photoelectrodes for Direct Solar Water Splitting”. We gratefully acknowledge John Turner, National Renewable Energy Lab, NREL, for his mentor- and leadership, both personally and for the overall PEC community. We further acknowledge the fruitful collaboration with AVANCIS GmbH, especially for supplying the sample used for taking the hitherto unpublished data in Fig. 5a, and P. Jackson and T. Friedlmeier (ZSW) for preparing the samples in Fig. 4.

Present address: [#]J.C.C.: Delaware Technical Community College, 400 Stanton Christiana Rd, Science Department, Newark, DE 19713, United States; james.carter@dtcc.edu

## REFERENCES


(1) Chen, Z.; Jaramillo, T. F.; Deutsch, T. G.; Kleiman-Shwarsctein, A.; Forman, A. J.; Gaillard, N.; Garland, R.; Takanabe, K.; Heske, C.; Sunkara, M.; et al. Accelerating Materials Development for Photoelectrochemical Hydrogen Production: Standards for Methods, Definitions, and Reporting Protocols. *J. Mater. Res.* **2010**, *25* (1), 3–16.

(2) Chen, Z.; Dinh, H. N.; Miller, E. *Photoelectrochemical Water Splitting – Standards, Experimental Methods, and Protocols*; Springer Briefs in Energy, 2013.

(3) Peerakiatkhajohn, P.; Yun, J.-H.; Wang, S.; Wang, L. Review of Recent Progress in Unassisted Photoelectrochemical Water Splitting: From Material Modification to Configuration Design. *J. Photonics Energy* **2016**, *7* (1), 012006.

(4) Li, X.; Zhao, L.; Yu, J.; Liu, X.; Zhang, X.; Liu, H.; Zhou, W. Water Splitting: From Electrode to Green Energy System. *Nano-Micro Lett.* **2020**, *12* (1), 131.

(5) Shay, J. L.; Wernick, J. H. *Ternary Chalcopyrite Semiconductors: Growth, Electronic Properties, and Applications*, 1st ed.; Pergamon, 1975.

(6) Peter, L. M. Photoelectrochemical Water Splitting. A Status Assessment. *Electroanalysis* **2015**, *27* (4), 864–871.

(7) Parkinson, B.; Turner, J. A. The Potential Contribution of Photoelectrochemistry in the Global Energy Future. In *Photoelectrochemical Water Splitting: Materials, Processes and Architectures*; The Royal Society of Chemistry, 2013.

(8) Panthani, M. G.; Akhavan, V.; Goodfellow, B.; Schmidtke, J. P.; Dunn, L.; Dodabalapur, A.; Barbara, P. F.; Korgel, B. A. Synthesis of $CuInS_2$, $CuInSe_2$, and $Cu(In_xGa_{1-x})Se_2$ (CIGS) Nanocrystal "Inks" for Printable Photovoltaics. *J. Am. Chem. Soc.* **2008**, *130* (49), 16770–16777.

(9) Green, M. A.; Dunlop, E. D.; Hohl-Ebinger, J.; Yoshita, M.; Kopidakis, N.; Bothe, K.; Hinken, D.; Rauer, M.; Hao, X. Solar Cell Efficiency Tables (Version 60). *Progress in Photovoltaics: Research and Applications* **2022**, *30* (7), 687–701. https://doi.org/10.1002/pip.3595.

(10) Bär, M.; Bohne, W.; Röhrich, J.; Strub, E.; Lindner, S.; Lux-Steiner, M. C.; Fischer, C.-H.; Niesen, T. P.; Karg, F. Determination of the Band Gap Depth Profile of the Penternary $Cu(In_{(1-X)}Ga_X)(S_YSe_{(1-Y)})_2$ Chalcopyrite from Its Composition Gradient. *J. Appl. Phys* **2004**, *96* (7), 3857–3860.

(11) Iranzo-Marín, F.; Debiemme-Chouvy, C.; Herlem, M.; Sculfort, J.-L.; Etcheberry, A. Electrochemical Techniques for the Elucidation of the Interface Structure of the N-InP/Aqueous Electrolyte Junction. *J. Electroanal. Chem.* **1994**, *365* (1), 283–287.

(12) Tauc, J. Optical Properties and Electronic Structure of Amorphous Ge and Si. *Mater. Res. Bull.* **1968**, *3* (1), 37–46.

(13) Schmid, D.; Ruckh, M.; Schock, H. W. Photoemission Studies on $Cu(In,Ga)Se_2$ Thin Films and Related Binary Selenides. *Appl. Surf. Sci.* **1996**, *103* (4), 409–429.

(14) Morkel, M.; Weinhardt, L.; Lohmüller, B.; Heske, C.; Umbach, E.; Riedl, W.; Zweigart, S.; Karg, F. Flat Conduction-Band Alignment at the $CdS/CuInSe_2$ Thin-Film Solar-Cell Heterojunction. *Appl. Phys. Lett.* **2001**, *79* (27), 4482–4484.

(15) Weinhardt, L.; Morkel, M.; Gleim, T.; Zweigart, S.; Niesen, T. P.; Karg, F.; Heske, C.; Umbach, E. Band Alignment at the $CdS/CuIn(S,Se)_2$ Heterojunction in Thin Film Solar Cells. In *Proceedings of the 17th EU PVSEC*; WIP-Renewable Energies: Munich, Germany, 2001; p 1261.

(16) Hauschild, D.; Handick, E.; Göhl-Gusenleitner, S.; Meyer, F.; Schwab, H.; Benkert, A.; Pohlner, S.; Palm, J.; Tougaard, S.; Heske, C.; et al. Band-Gap Widening at the Cu(In,Ga)(S,Se)$_2$ Surface: A Novel Determination Approach Using Reflection Electron Energy Loss Spectroscopy. *ACS Appl. Mater. Interfaces* **2016**, *8* (32), 21101–21105.
(17) Heske, C.; Weinhardt, L.; Bär, M. X-Ray and Electron Spectroscopy Studies of Oxide Semiconductors for Photoelectrochemical Hydrogen Production. *On Solar Hydrogen and Nanotechnology* **2010**, 143.
(18) Smith, N. V. Inverse Photoemission. *Rep. Prog. Phys.* **1988**, *51* (9), 1227–1294.
(19) Weinhardt, L.; Hauschild, D.; Heske, C. Surface and Interface Properties in Thin-Film Solar Cells: Using Soft X-Rays and Electrons to Unravel the Electronic and Chemical Structure. *Adv. Mater.* **2019**, *31* (26), 1806660.
(20) Nozik, A. J.; Memming, R. Physical Chemistry of Semiconductor−Liquid Interfaces. *J. Phys. Chem.* **1996**, *100* (31), 13061–13078.
(21) Nelson, J. *The Physics of Solar Cells*, 1st ed.; Imperial College Press, 2003.
(22) Babbe, F.; Choubrac, L.; Siebentritt, S. Quasi Fermi Level Splitting of Cu-Rich and Cu-Poor Cu(In,Ga)Se$_2$ Absorber Layers. *Appl. Phys. Lett.* **2016**, *109* (8), 082105.
(23) Schuler, S.; Siebentritt, S.; Nishiwaki, S.; Rega, N.; Beckmann, J.; Brehme, S.; Lux-Steiner, M. Ch. Self-Compensation of Intrinsic Defects in the Ternary Semiconductor CuGaSe$_2$. *Phys. Rev. B* **2004**, *69* (4), 045210.
(24) Hu, X.; Xue, J.; Tian, J.; Weng, G.; Chen, S. Effect of Cu/Ga Ratio on Deep-Level Defects in CuGaSe$_2$ Thin Films Studied by Photocapacitance Measurements with Two-Wavelength Excitation. *Appl. Opt.* **2017**, *56* (14), 4090–4094.
(25) Khan, I. S.; Muzzillo, C. P.; Perkins, C. L.; Norman, A. G.; Young, J. L.; Gaillard, N.; Zakutayev, A. Mg$_x$Zn$_{1-x}$O Contact to CuGa$_3$Se$_5$ Absorber for Photovoltaic and Photoelectrochemical Devices. *J. Phys. Energy* **2021**, *3* (2), 024001.
(26) Weinhardt, L.; Fuchs, O.; Peter, A.; Umbach, E.; Heske, C.; Reichardt, J.; Bär, M.; Lauermann, I.; Kötschau, I.; Grimm, A.; et al. Spectroscopic Investigation of the Deeply Buried Cu(In,Ga)(S,Se)$_2$/Mo Interface in Thin-Film Solar Cells. *J. Chem. Phys.* **2006**, *124* (7), 074705-074705–5.
(27) Weinhardt, L.; Blum, M.; Bär, M.; Heske, C.; Fuchs, O.; Umbach, E.; Denlinger, J. D.; Ramanathan, K.; Noufi, R. Chemical Properties of the Cu(In,Ga)Se$_2$/Mo/Glass Interfaces in Thin Film Solar Cells. *Thin Solid Films* **2007**, *515* (15), 6119–6122.
(28) Bär, M.; Weinhardt, L.; Heske, C.; Nishiwaki, S.; Shafarman, W. N. Chemical Structures of the Cu(In,Ga)Se$_2$/Mo and Cu(In,Ga)(S,Se)$_2$/Mo Interfaces. *Phys. Rev. B* **2008**, *78* (7), 075404.
(29) Bär, M.; Nishiwaki, S.; Weinhardt, L.; Pookpanratana, S.; Shafarman, W. N.; Heske, C. Electronic Level Alignment at the Deeply Buried Absorber/Mo Interface in Chalcopyrite-Based Thin Film Solar Cells. *Appl. Phys. Lett.* **2008**, *93* (4), 042110-042110–042113.
(30) Probst, V.; Stetter, W.; Riedl, W.; Vogt, H.; Wendl, M.; Calwer, H.; Zweigart, S.; Ufert, K.-D.; Freienstein, B.; Cerva, H.; et al. Rapid CIS-Process for High Efficiency PV-Modules: Development towards Large Area Processing. *Thin Solid Films* **2001**, *387* (1–2), 262–267.
(31) Jackson, P.; Hariskos, D.; Wuerz, R.; Wischmann, W.; Powalla, M. Compositional Investigation of Potassium Doped Cu(In,Ga)Se$_2$ Solar Cells with Efficiencies up to 20.8%. *Phys. Status Solidi RRL* **2014**, *8* (3), 219–222.

(32) Jackson, P.; Hariskos, D.; Wuerz, R.; Kiowski, O.; Bauer, A.; Friedlmeier, T. M.; Powalla, M. Properties of Cu(In,Ga)$Se_2$ Solar Cells with New Record Efficiencies up to 21.7%. *phys. stat. sol. (RRL)* **2015**, *9* (1), 28–31.
(33) Hauschild, D.; Kreikemeyer-Lorenzo, D.; Jackson, P.; Friedlmeier, T. M.; Hariskos, D.; Reinert, F.; Powalla, M.; Heske, C.; Weinhardt, L. Impact of a RbF Postdeposition Treatment on the Electronic Structure of the CdS/Cu(In,Ga)$Se_2$ Heterojunction in High-Efficiency Thin-Film Solar Cells. *ACS Energy Lett.* **2017**, *2* (10), 2383–2387.
(34) Friedlmeier, T. M.; Jackson, P.; Kreikemeyer-Lorenzo, D.; Hauschild, D.; Kiowski, O.; Hariskos, D.; Weinhardt, L.; Heske, C.; Powalla, M. A Closer Look at Initial CdS Growth on High-Efficiency Cu(In,Ga)$Se_2$ Absorbers Using Surface-Sensitive Methods. In *Proc. of the 2016 IEEE 43rd Photovoltaic Specialists Conference (PVSC)*; IEEE, Piscataway, NJ: Portland, Oregon, USA, 2016; pp 0457–0461.
(35) Kreikemeyer-Lorenzo, D.; Hauschild, D.; Jackson, P.; Friedlmeier, T. M.; Hariskos, D.; Blum, M.; Yang, W.; Reinert, F.; Powalla, M.; Heske, C.; et al. Rubidium Fluoride Post-Deposition Treatment: Impact on the Chemical Structure of the Cu(In,Ga)$Se_2$ Surface and CdS/Cu(In,Ga)$Se_2$ Interface in Thin-Film Solar Cells. *ACS Appl. Mater. Interfaces* **2018**, *10* (43), 37602.
(36) Stölzel, M.; Algasinger, M.; Zelenia, A.; Weber, A.; Sode, M.; Schubbert, C.; Eraerds, P.; Lechner, R.; Dalibor, T.; Palm, J. Absorber Optimization in CIGSSe Modules with a Sputtered ZnOS Buffer Layer at 19% Efficiency. In *Proceedings of the 36th EU PVSEC*; WIP Renewable Energies: Marseille, France, 2019; pp 590–596.
(37) Weinhardt, L.; Fuchs, O.; Groß, D.; Storch, G.; Umbach, E.; Dhere, N. G.; Kadam, A. A.; Kulkarni, S. S.; Heske, C. Band Alignment at the CdS/Cu(In,Ga)$S_2$ Interface in Thin-Film Solar Cells. *Appl. Phys. Lett.* **2005**, *86* (6), 062109-062109–3.
(38) Weinhardt, L.; Fuchs, O.; Groß, D.; Umbach, E.; Heske, C.; Dhere, N. G.; Kadam, A. A.; Kulkarni, S. S. Surface Modifications of Cu(In,Ga)$S_2$ Thin Film Solar Cell Absorbers by KCN and $H_2O_2$/$H_2SO_4$ Treatments. *J. Appl. Phys* **2006**, *100* (2), 024907-024907–4.
(39) Bär, M.; Schubert, B.-A.; Marsen, B.; Krause, S.; Pookpanratana, S.; Unold, T.; Weinhardt, L.; Heske, C.; Schock, H.-W. Impact of KCN Etching on the Chemical and Electronic Surface Structure of $Cu_2ZnSnS_4$ Thin-Film Solar Cell Absorbers. *Appl. Phys. Lett.* **2011**, *99* (15), 152111.
(40) Gaillard, N.; Prasher, D.; Chong, M.; Deangelis, A.; Horsley, K.; Ishii, H. A.; Bradley, J. P.; Varley, J.; Ogitsu, T. Wide-Bandgap Cu(In,Ga)$S_2$ Photocathodes Integrated on Transparent Conductive F:$SnO_2$ Substrates for Chalcopyrite-Based Water Splitting Tandem Devices. *ACS Appl. Energy Mater.* **2019**, *2* (8), 5515–5524.
(41) Seah, M. P.; Briggs, D. *Practical Surface Analysis: Auger and X-Ray Photoelectron Spectroscopy*, 1st ed.; John Wiley & Sons Ltd: Chichester ; New York : Aarau, 1990.
(42) Trasatti, S. The Absolute Electrode Potential: An Explanatory Note (Recommendations 1986). *Pure Appl. Chem.* **1986**, *58* (7), 955–966.
(43) Heske, C.; Fink, R.; Umbach, E.; Riedl, W.; Karg, F. Surface Preparation Effects of Polycrystalline Cu(In,Ga)$Se_2$ Thin Films Studied by XPS and UPS. *Cryst. Res. Technol.* **1996**, *31* (919), 919–922.
(44) Rietwyk, K. J.; Keller, D. A.; Ginsburg, A.; Barad, H.-N.; Priel, M.; Majhi, K.; Yan, Z.; Tirosh, S.; Anderson, A. Y.; Ley, L.; et al. Universal Work Function of Metal Oxides Exposed to Air. *Adv. Mater. Interfaces* **2019**, *6* (12), 1802058.
(45) Wang, J. *Analytical Electrochemistry*, 3rd ed.; Wiley-VCH: Hoboken, N.J, 2006.

(46) Pourbaix, M. *Atlas of Electrochemical Equilibria in Aqueous Solutions*; National Association of Corrosion Engineers: Houston, Texas, USA, 1974.
(47) Turner, J. A. Energetics of the Semiconductor-Electrolyte Interface. *J. Chem. Educ.* **1983**, *60* (4), 327.
(48) Memming, R. Solar Energy Conversion by Photoelectrochemical Processes. *Electrochimica Acta* **1980**, *25* (1), 77–88.
(49) Mezher, M.; Garris, R.; Mansfield, L. M.; Blum, M.; Hauschild, D.; Horsley, K.; Duncan, D. A.; Yang, W.; Bär, M.; Weinhardt, L.; et al. Soft X-Ray Spectroscopy of a Complex Heterojunction in High-Efficiency Thin-Film Photovoltaics: Intermixing and Zn Speciation at the Zn(O,S)/Cu(In,Ga)$Se_2$ Interface. *ACS Appl. Mater. Interfaces* **2016**, *8* (48), 33256–33263.
(50) Weinhardt, L.; Fuchs, O.; GroB, D.; Storch, G.; Dhere, N. G.; Kadam, A. A.; Kulkarni, S. S.; Visbeck, S.; Niesen, T. P.; Karg, F.; Heske, C.; Umbach, E. Comparison of Band Alignments at Various CdS/Cu(In,Ga)$(S,Se)_2$ Interfaces in Thin Film Solar Cells. In *Proceedings of the 4th World Conference on Photovoltaic Energy Conversion (WCPEC-4)*; IEEE Electron Devices Society: Waikoloa, HI, USA, 2006; Vol. 1, pp 412–415.
(51) Weinhardt, L.; Blum, M.; Bär, M.; Heske, C.; Cole, B.; Marsen, B.; Miller, E. L. Electronic Surface Level Positions of $WO_3$ Thin Films for Photoelectrochemical Hydrogen Production. *J. Phys. Chem. C* **2008**, *112* (8), 3078–3082.
(52) Chun, W.-J.; Ishikawa, A.; Fujisawa, H.; Takata, T.; Kondo, J. N.; Hara, M.; Kawai, M.; Matsumoto, Y.; Domen, K. Conduction and Valence Band Positions of $Ta_2O_5$, TaON, and $Ta_3N_5$ by UPS and Electrochemical Methods. *J. Phys. Chem. B* **2003**, *107* (8), 1798–1803.
(53) Bär, M.; Weinhardt, L.; Marsen, B.; Cole, B.; Gaillard, N.; Miller, E.; Heske, C. Mo Incorporation in $WO_3$ Thin Film Photoanodes: Tailoring the Electronic Structure for Photoelectrochemical Hydrogen Production. *Appl. Phys. Lett.* **2010**, *96* (3), 032107.
(54) Gleim, T.; Heske, C.; Umbach, E.; Schumacher, C.; Faschinger, W.; Ammon, C.; Probst, M.; Steinrück, H.-P. Reduction of the ZnSe/GaAs(100) Valence Band Offset by a Te Interlayer. *Appl. Phys. Lett.* **2001**, *78* (13), 1867–1869.
(55) Gleim, T.; Heske, C.; Umbach, E.; Schumacher, C.; Gundel, S.; Faschinger, W.; Fleszar, A.; Ammon, C.; Probst, M.; Steinrück, H.-P. Formation of the ZnSe/(Te/)GaAs(100) Heterojunction. *Surf. Sci.* **2003**, *531* (1), 77–85.
(56) Morkel, M. Elektronenspektroskopie Zur Direkten Bestimmung Des Leitungsbandoffsets in Dünnschichtsolarzellen: Die Reale CdS/Cu(In,Ga)$(S,Se)_2$ Grenzfläche. Diploma Thesis, University of Würzburg, Würzburg, 2000.
(57) Jaffe, J. E.; Zunger, A. Theory of the Band-Gap Anomaly in $ABC_2$ Chalcopyrite Semiconductors. *Phys. Rev. B* **1984**, *29* (4), 1882–1906.
(58) Weinhardt, L. Elektronenspektroskopische Untersuchungen an Grenzflächen Und Oberflächen in Cu(In,Ga)$(S,Se)_2$ Dünnschichtsolarzellen. Diploma Thesis, University of Würzburg, Würzburg, 2001.
(59) *New efficiency record for CIGS solar modules*. AVANCIS. https://www.avancis.de/en/avancis-achieves-new-efficiency-record-for-cigs-solar-modules/ (accessed 2022-05-04).
(60) Pettersson, J.; Platzer-Björkman, C.; Zimmermann, U.; Edoff, M. Baseline Model of Graded-Absorber Cu(In,Ga)$Se_2$ Solar Cells Applied to Cells with $Zn_{1-x}Mg_xO$ Buffer Layers. *Thin Solid Films* **2011**, *519* (21), 7476–7480.

(61) Jackson, P.; Wuerz, R.; Hariskos, D.; Lotter, E.; Witte, W.; Powalla, M. Effects of Heavy Alkali Elements in Cu(In,Ga)$Se_2$ Solar Cells with Efficiencies up to 22.6%. *Phys. Status Solidi RRL* **2016**, *10* (8), 583–586.
(62) Heske, C.; Fink, R.; Umbach, E.; Riedl, W.; Karg, F. Electronic and Compositional Effects of Na Deposition on Cu(In,Ga)$Se_2$ Thin Film Surfaces. *Cryst. Res. Technol.* **1996**, *31* (465).
(63) Heske, C.; Richter, G.; Chen, Z.; Fink, R.; Umbach, E.; Riedl, W.; Karg, F. Influence of Na and $H_2O$ on the Surface Properties of Cu(In,Ga)$Se_2$ Thin Films. *J. Appl. Phys.* **1997**, *82* (5), 2411.
(64) Karthikeyan, S.; Hwang, S.; Sibakoti, M.; Bontrager, T.; Liptak, R. W.; Campbell, S. A. Effect of Rapid Thermal Annealing of Copper Indium Aluminium Gallium Diselenide Solar Cell Devices and Its Deposition Challenges. *Appl. Surf. Sci.* **2019**, *493*, 105–111.
(65) Valdes, N.; Lee, J.; Shafarman, W. Ag Alloying and KF Treatment Effects on Low Bandgap CIGS Solar Cells. In *Proceedings of the 7th World Conference on Photovoltaic Energy Conversion (WCPEC-7)*; IEEE Electron Devices Society: Waikoloa, HI, USA, 2018; pp 1652–1654.
(66) Varley, J. B.; Lordi, V.; Ogitsu, T.; Deangelis, A.; Horsley, K.; Gaillard, N. Assessing the Role of Hydrogen in Fermi-Level Pinning in Chalcopyrite and Kesterite Solar Absorbers from First-Principles Calculations. *J. Appl. Phys* **2018**, *123* (16), 161408.
(67) Weinhardt, L.; Heske, C.; Umbach, E.; Niesen, T. P.; Visbeck, S.; Karg, F. Band Alignment at the I-ZnO/CdS Interface in Cu(In,Ga)$(S,Se)_2$ Thin-Film Solar Cells. *Appl. Phys. Lett.* **2004**, *84* (16), 3175–3177.
(68) Duncan, D. A.; Mendelsberg, R.; Mezher, M.; Horsley, K.; Rosenberg, S. G.; Blum, M.; Xiong, G.; Weinhardt, L.; Gloeckler, M.; Heske, C. A New Look at the Electronic Structure of Transparent Conductive Oxides—A Case Study of the Interface between Zinc Magnesium Oxide and Cadmium Telluride. *Adv. Mater. Interfaces* **2016**, *3* (22), 1600418.

TOC Graphic

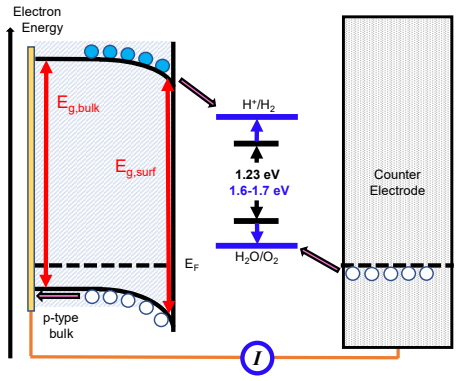
Electron
Energy
$E_{g,bulk}$
$E_{g,surf}$
$E_F$
p-type
bulk
$H^+/H_2$
1.23 eV
1.6-1.7 eV
$H_2O/O_2$
Counter
Electrode
I